J Mol Model (2011) 17:701–708
DOI 10.1007/s00894-010-0766-9

ORIGINAL PAPER

Computational characterization of sodium selenite using density functional theory

Diana Barraza-Jiménez · Manuel Alberto Flores-Hidalgo · Donald H. Galvan · Esteban Sánchez · Daniel Glossman-Mitnik

Received: 10 February 2010 / Accepted: 20 May 2010 / Published online: 9 June 2010

Abstract In this theoretical study we used density functional theory to calculate the molecular and crystalline structures of sodium selenite. Our structural results were compared with experimental data. From the molecular structure we determined the ionization potential, electronic affinity, and global reactivity parameters like electronegativity, hardness, softness and global electrophilic index. A significant difference in the IP and EA values was observed, and this difference was dependent on the calculation method used (employing either vertical or adiabatic energies). Thus, values obtained for the electrophilic index (2.186 eV from vertical energies and 2.188 eV from adiabatic energies) were not significantly different. Selectivity was calculated using the Fukui functions. Since the Mulliken charge study predicted a negative value, it is recommended that AIM should be used in selectivity characterization. It was evident from the selectivity index that sodium atoms are the most sensitive sites to nucleophilic attack. The results obtained in this work provide data that will aid the characterization of compounds used in crop biofortification.

D. Barraza-Jiménez (✉) · E. Sánchez
Centro de Investigación en Alimentación y Desarrollo,
A.C. Unidad Delicias,
Av. 4ª Sur 3820, Fracc. Vencedores del Desierto. Cd,
Delicias Chih, México 33089
e-mail: dbarraza@ciad.mx

M. A. Flores-Hidalgo · D. Glossman-Mitnik
Centro de Investigación en Materiales Avanzados,
S.C., M. de Cervantes 120, Complejo Industrial Chihuahua,
Chihuahua Chih, México 31109

D. H. Galvan
Centro de Nanociencias y Nanotecnología-Universidad Nacional
Autónoma de México,
Carretera Tijuana-Ensenada Km 107. Ensenada,
Baja California, México 22800

Keywords Molecular structure sodium selenite · Crystal structure sodium selenite · Global electrophilic index · Fukui functions · Biofortification

Introduction

Anhydrous sodium selenite (Na_2SeO_3) is an important inorganic species that is used in a variety of biological applications, such as in biofortification programs. Na_2SeO_3 is one of the compounds that allows selenium to be easily taken up by plants [1]. Plants and animals absorb Se through this inorganic compound, and it is known that Se is an essential micronutrient for many organisms, including plants, animals and humans [2]. Furthermore, Se is very important for human health, being involved (mainly through the activity of selenoenzymes) in antioxidant, anti-inflammatory, anticancer, antiheart disease, antiviral, and antiaging activities, as well as in fertility, thyroid, brain and immune functions [3]. In addition, Se is important in mammalian nutrition, since Se deficiency may promote cancer [4]. Dietary Se deficiency in humans is caused by the ingestion of plant foods with negligible concentrations of this element, due to its low bioavailability in most crop soils [5, 6] from various parts of the world, such as China, UK, Eastern Europe, Africa, and Australia [7, 8].

Several teams have studied Na_2SeO_3; for example, Kamal et al. [9] gave sodium selenate and Na_2SeO_3 as supplements to poultry and livestock feed to promote growth and prevent selenium deficiency diseases. They performed a thirteen-week toxicity study focusing on water consumption in mice that has biological applications. Some other teams have used Na_2SeO_3 in other biological applications [10, 11]. Xi Li et al. [12] studied the effect of Na_2SeO_3 on the mitochondrial metabolism of *Carassius auratus* liver, and proposed that the

microcalorimetric method is a straightforward and simple method to use in studies of mitochondria; their work, together with that of several other teams, has biotechnological applications [13, 14]. From a chemical perspective, Sumiko et al. [15] investigated the photocatalytic reduction of selenate and selenite solutions using TiO_2 powders, and used Na_2SeO_3 to obtain Se with this method.

Regarding computational studies, different inorganic salts have been studied using computational methods such as density functional theory, as implemented in the CASTEP code and with the PW91 functional [16–18]. Among these are studies of calcium selenide CaSe and BaSe [19, 20] in crystals such as $BaWO_4$. The computational results obtained approximated experimental results well [21]. We evaluated some other works related to chemical applications of sodium selenite [22–25]. One problem that we noted is that information on the characterization of Na_2SeO_3 is scarce. Experimental data, such as that of Wickleder [26], who presented Na_2SeO_3 crystallographic data, are rather rare. We used the latter work as an experimental reference to compare with our theoretical results.

To the best of our knowledge, theoretical studies related to the structure of Na_2SeO_3 and its reactivity parameters are unavailable. On the other hand, for molecular structure data, the HCTH functional was used to study sulfur compounds, and this achieved the closest geometries to those reported in experimental studies [27]. Since the chemical properties of selenium and sulfur, as well as their electronegativities, are very similar, HCTH 407 was selected for Na_2SeO_3 molecular structure calculations. In the present theoretical study, we used density functional theory (DFT) to calculate the crystalline and molecular structures of sodium selenite. Our structural results were compared with experimental crystallographic data. From the molecular structure we determined the ionization potential (IP), electronic affinity (EA), and global reactivity parameters like electronegativity, hardness, softness, and global electrophilic index. Selectivity was calculated using the Fukui functions. The results obtained in this work provide data that will aid the characterization of compounds used in crop biofortification. We provide electronic structure data for sodium selenite that will facilitate the characterization of new compounds used as nutrients in plant biofortification.

Computational details

Geometric optimization of sodium selenite in its crystal form was done using density functional theory (DFT) [28, 29], utilizing a plane wave as implemented in the Cambridge Serial Total Energy Package (CASTEP) [30], which treats crystals as periodic systems. The Broyden, Fletcher, Goldfarb and Shanno (BFGS) method [31–34] was applied to optimize the model structure in the reciprocal space. We used the generalized gradient approach (GGA) functional and the gradient-corrected functional PW91 by Perdew and Wang [35], as it has been suggested that PW91 is the best option to enable a comparison of the calculated results with those in the literature [36]. We used a cutoff energy of 410 eV with ultrasoft pseudo-potentials [37]. The crystalline structure was calculated with the Materials Studio software [38], which provided a way to compare the calculated results with experimentally derived parameters.

After the geometry had been optimized in CASTEP, we changed the structure to its molecular form in order to compute the reactivity and selectivity parameters, and the ground-state geometry of sodium selenite was evaluated using the Gaussian 03 software package [39]. The HCTH 407 functional [40, 41] was employed for this purpose. This functional can obtain thermochemical data with good precision for inorganic systems [42]. It was used in combination with the DGDZVP (density Gaussian double-zeta with polarization functions) basis set [43], which can be utilized for a vast variety of different atomic species. This was approximated to 6–31+G*, and gave the same quality of results as TZVP [44].

Vibrational frequencies were obtained at the same level used for the geometric optimization, and this allowed us to verify that the stationary points found are local minima of the potential energy surface. The Fukui functions [45] were calculated using Mulliken population analysis [46, 47] and the atoms in molecules (AIM) theory [48].

Results and discussion

The crystal structure is shown in Fig. 1. After the geometric optimization, we calculated the relative error by comparing

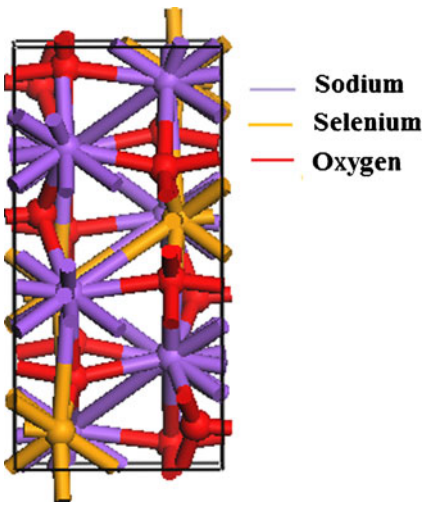

Fig. 1 Crystal structure of sodium selenite obtained using the CASTEP PW91 functional

Table 1 Bond length data (Å) for crystalline sodium selenite

Bond	Theoretical length[a]	Experimental length[b]	% Relative error
Na(1)–O(1)	2.495	2.519	0.934
Na(1)–O(1)	2.818	2.650	6.338
Na(1)–O(2)	2.428	2.408	0.860
Na(1)–O(2)	2.692	2.657	1.328
Na(1)–O(3)	2.375	2.346	1.224
Na(1)–O(3)	2.395	2.373	0.937
Na(2)–O(1)	2.469	2.438	1.256
Na(2)–O(1)	2.647	2.664	0.650
Na(2)–O(2)	2.504	2.473	1.283
Na(2)–O(2)	2.441	2.390	2.138
Na(2)–O(3)	2.396	2.355	1.756
Na(2)–O(1)	2.551	2.516	1.385
Se(1)–O(1)	1.720	1.703	1.003
Se(1)–O(2)	1.720	1.705	0.844
Se(1)–O(3)	1.706	1.685	1.220

[a] Theoretical data obtained using CASTEP with PW91

[b] Experimental data [26]

our results with experimental data. The calculated bond lengths, those obtained from experimental data, and the relative errors between them are shown in Table 1. Relative error between experimental and our theoretical results for Na-O bond length presents values between 0.65% and 2.130% except bond length relative error for Na(1)-O(1). These small errors show that our theoretical method is acceptable.

Experimental data for crystalline sodium selenite indicate a monoclinic structure belonging to the P21/c spatial group, with lattice parameters a=4.9089 Å, b=10.0072 Å, c=6.8535 Å, β= 91.11 Å. In contrast, our theoretical results are a=4.9634 Å, b= 10.1311 Å, c=7.0061 Å, β=89.9524 Å. When the experimental and theoretical crystal parameters are compared, a maximum error of 2.22% is found for the c parameter. This small error for the first theoretical calculation indicated that our results are acceptable for a first theoretical approximation.

In Table 2, we show the bond length parameters and bond angles for the molecular structure of sodium selenite. The bond lengths for Na(1)–O(1) and Na(2)–O(3) were the same, while those for Na(2)–O(2) and Na(1)–O(2), which correspond to O(2), are on average 2.247 Å. The Se–O bond length ranges from 1.718 Å for Se–O(1) and Se–O(3) to 1.810 Å for Se–O(2).

Likewise, the bond angles are similar for O(1)–Se–O(2) and O(2)–Se–O(3). On the other hand, the angle O(1)–Se–O(3) is 8.9° larger than those just mentioned.

Energies

Neutral, cationic and anionic energies were calculated by both adiabatic and vertical energy methods. Our results for the energies, ionization potentials and electronic affinities are shown in Table 3.

For sodium selenite, we calculated an ionization potential of 7.605 eV using vertical energies and 7.108 eV using adiabatic energies; the difference between these values is 0.497 eV.

This difference in the ionization potentials obtained using vertical and adiabatic energies indicates that there is a significant decrease in the IP (around 0.5 eV) after

Table 2 Interatomic bond distances (Å) and bond angles (°) for sodium selenite

Bond	Theoretical length (Å)	Bond angle	Theoretical angle (°)
Na(1)–Na(2)	4.014	Na(1)–Na(2)–Se	45.9
Na(1)–O(1)	2.202	Na(1)–Na(2)–O(3)	74.0
Na(1)–O(2)	2.247	Na(1)–O(1)–Se	94.0
Na(2)–Se	2.887	Na(1)–O(2)–Se	90.1
Na(2)–O(1)	4.011	O(1)–Na(2)–O(2)	40.0
Na(2)–O(2)	2.246	O(1)–Na(2)–O(3)	42.1
Na(2)–O(3)	2.202	O(1)–Se–O(2)	100.2
Se–O(1)	1.718	O(1)–Se–O(3)	109.1
Se(1)–O(2)	1.810	O(2)–Se–O(3)	100.2
Se–O(3)	1.718	O(2)–Na(2)–O(3)	75.0

Theoretical data obtained using the DFT HCTH407 functional and the DGDZVP basis set

Experimental data are unavailable

Table 3 Neutral, cationic and anionic energies (u.a.) and IP and EA (eV) values for sodium selenite

Method	Neutral	Cationic	Anionic	IP	EA
Vertical energies	−2952.620	−2952.341	−2952.634	7.605	0.356
Adiabatic energies	−2952.620	−2952.359	−2952.639	7.108	0.498

Theoretical data obtained using the DFT HCTH407 functional and the DGDZVP basis set
Experimental data are unavailable

geometric optimization and the cationic and anionic energies have been calculated.

For the electronic affinity, we obtained a value of 0.356 eV when calculated using vertical energies and 0.498 eV when using adiabatic energies; the difference between these values is 0.142 eV.

Table 3 shows that the anionic and cationic energies calculated using the adiabatic energy method are lower than those calculated using the vertical energy method, which is why we consider the adiabatic energy method to give the best approximation (minimum energy).

Reactivity parameters

The frontier orbitals HOMO and LUMO allow us to get a first approximation of the reactivity. However, the results presented here should be considered with caution, because frontier molecular orbital theory is known to give inaccurate results in certain cases, and it is not commonly applied to the study of inorganic salts. Figure 2 shows how the HOMO density extends through the SeO_3 radical, where the selenium atom does not present negative diffusivity towards the oxygen atoms. The LUMO orbital is found on the sodium atoms and creates a positive environment.

Other parameters related to the reactivity, such as softness, global hardness, electronegativity and global electrophilic index, were calculated using the vertical and adiabatic energy methods, just as for the IP and EA calculations.

There is a study that proposes that the chemical potential corresponds to the electronegativity but with the opposite sign [49]. We calculated the electronegativity to determine how far the energy drops when an infinitesimal amount of electronic charge enters the molecular system. Considering that electrons flow from a high chemical potential to a low chemical potential until the system reaches equilibrium, we can calculate the electronegativity using Eq. 1:

$$\chi = \frac{1}{2}(IP + EA), \tag{1}$$

where χ represents the electronegativity, IP is the ionization potential, and EA is the electronic affinity.

The electronegativity value obtained from the vertical energies was 3.980 eV, and that obtained from the adiabatic energies was 3.803 eV; these values differ by 0.177 eV.

Global hardness measures the molecule's resistance to a change in the electronic distribution [38], and this can be calculated with Eq. 2:

$$\eta = \frac{1}{2}(IP - EA) \tag{2}$$

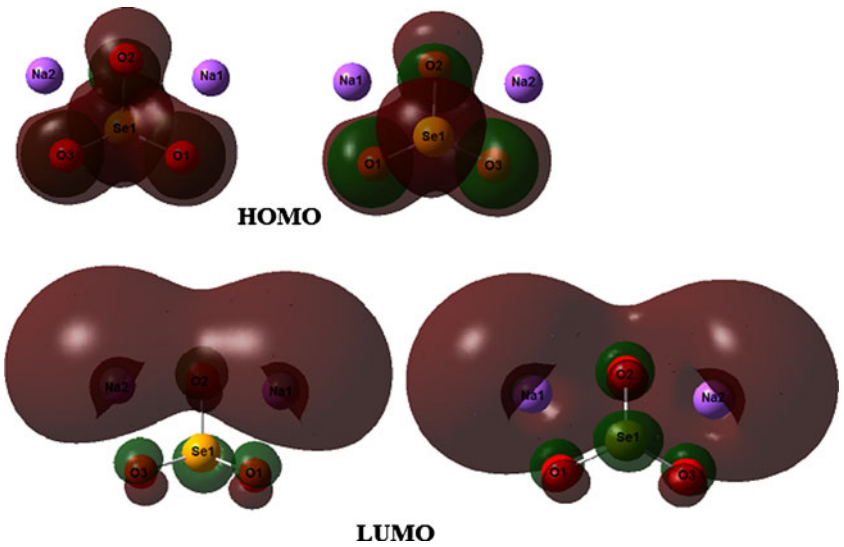

Fig. 2a–b Frontier orbitals for sodium selenite: HOMO and LUMO, obtained with the DFT HCTH functional and the DGDZVP basis set

Table 4 Condensed Fukui functions obtained using Mulliken charges and AIM for sodium selenite

Atom	Fukui function	Mulliken charge	Δf_x [a]	AIM	Δf_x [b]
Na(1)	f_x^+	0.463	0.286	0.433	0.378
	f_x^-	0.177		0.055	
	f_x^0	0.320		0.244	
Na(2)	f_x^+	0.481	0.305	0.449	0.394
	f_x^-	0.176		0.055	
	f_x^0	0.329		0.252	
Se(1)	f_x^+	0.070	−0.107	0.041	−0.108
	f_x^-	0.177		0.149	
	f_x^0	0.124		0.095	
O(1)	f_x^+	0.007	−0.175	0.025	−0.241
	f_x^-	0.182		0.266	
	f_x^0	0.095		0.146	
O(2)	f_x^+	−0.027	−0.131	0.027	−0.180
	f_x^-	0.104		0.207	
	f_x^0	0.039		0.117	
O(3)	f_x^+	0.006	−0.177	0.025	−0.242
	f_x^-	0.183		0.267	
	f_x^0	0.094		0.146	

Theoretical data obtained using the DFT HCTH407 functional and the DGDZVP basis set
[a] with Mulliken charges and [b] AIM

Here, the value obtained with vertical energies was 3.6244 eV and that obtained with adiabatic energies was 3.305 eV; these values differ by 0.319 eV.

Global softness quantifies the ability of a system to accept more electrons, and this can be calculated as the inverse of the hardness [50] using Eq. 3:

$$\sigma = \frac{1}{\eta} = 2\frac{1}{(IP - EA)} \tag{3}$$

Using the vertical and adiabatic energy methods, we obtained global hardnesses of 0.276 eV and 0.303 eV, respectively. These values differ by 0.027 eV.

Another indicator of the reactivity of a system is the global electrophilic index, which measures the system's energetic stability when saturated with electrons from an external medium. This can be calculated using Eq. 4:

$$\omega = \frac{\mu^2}{2\eta} \tag{4}$$

where ω is the global electrophilic index, μ^2 is the square of the chemical potential, and η is the global hardness. Vertical energies yielded a global electrophilic index of 2.186 eV and adiabatic energies gave an index of 2.188 eV; these values are almost identical.

Selectivity parameters

The condensed Fukui functions are local properties that represent the sensitivity of the chemical potential in the Kohn–Sham equations to external perturbations.

The following equations show the condensed Fukui functions for the molecule:

$$f_x^- = [q_x(N) - q_x(N-1)] \tag{5}$$

$$f_x^+ = [q_x(N+1) - q_x(N)] \tag{6}$$

$$f_x^0 = \frac{1}{2}\left[f_x^- + f_x^+\right] = \frac{1}{2}[q_x(N+1) - q_x(N-1)] \tag{7}$$

Equations 5, 6 and 7 can be used to calculate the sites of electrophilic, nucleophilic and radical attack, respectively.

Table 4 shows the condensed Fukui functions obtained using Mulliken charges (see the third column) and AIM

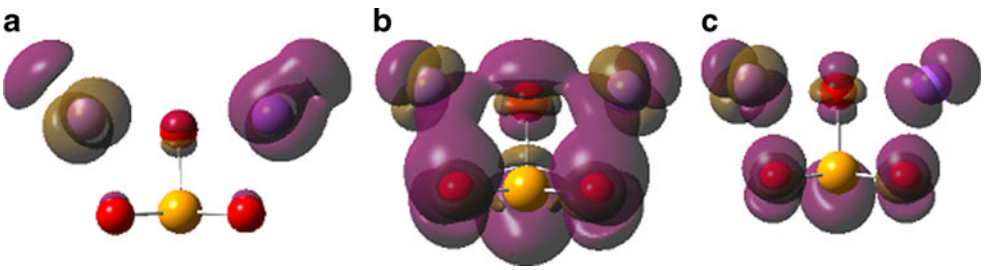

Fig. 3a–c Uncondensed Fukui functions of sodium selenite: **a** electrophilic Fukui function; **b** nucleophilic Fukui function; **c** radical Fukui function

(see the fifth column). The fourth and sixth columns of the table (Δf_x) correspond to the difference $\left(f_x^+ - f_x^-\right)$.

It is evident that sodium atoms provide the sites that are the most sensitive to nucleophilic attack. This conclusion is based on the selectivity index $\Delta f_x = f_x^+ - f_x^-$, because if the index is bigger than zero the site will be electrophilic, which is the case for Na(1) and Na(2) since these are the only values with positive Δf_x. Here, the electrophilic index value is bigger for Na(2) than for Na (1). Oxygen and selenium atoms show negative selectivity indices, which means that they are nucleophilic sites; their nucleophilicities increase according to the series Se < O(2) < O(1), O(3).

Upon considering Mulliken charge versus AIM, we noted that the sodium atoms showed the most variation in values because a different population charge analysis was used for them. Selenium did not show significant changes in Δf_x, but the oxygen atoms exhibited a dependence on the type of charge analysis employed. O(2) was the oxygen atom that showed the least dependence on Mulliken charge or AIM, which can be attributed to the fact that the f_x^+ function for O (2) was negative, which means that it does not have physical meaning.

According to the f_x^0 function, the sodium atoms are the most likely to be radical sites, followed by the oxygen atoms, and then O(2); finally, selenium has the lowest value for the Fukui function, and so is least likely to act as a radical within the molecule.

Even though both analyses, Mulliken and AIM, showed similar trends for the three different functions with the different atoms, we can see that for sodium and selenium the Fukui functions gave higher values when Mulliken charges were used. The opposite was true for the three oxygen atoms, since $f_x^+, f_x^- y f_x^0$ increased when AIM was used.

Figure 3 shows the uncondensed Fukui functions for electrophilic, nucleophilic and radical attack. Nucleophilic attack will take place at positively charged atoms. For instance, the sodium atoms had positive charges, as expected, but there was a stronger diffusion of negative charge around the Na(2) atom, probably due to the compound's electronic delocalization. For electrophilic attack, the highest intensity was detected around the oxygen atoms, followed by selenium. Finally, the radical site representation is in agreement with the order described in Table 4: Na(2) > Na(1) > O(1), O(3) > Se.

Conclusions

The molecular and crystalline structures of sodium selenite were characterized using DTF computational calculations, and the data obtained approximated well to the crystalline structure derived experimentally by other research groups. The crystalline structure results were the basis for our molecular characterization.

We observed a significant difference between the IP and EA values for this compound, and the difference was dependent on the calculation method (using either vertical or adiabatic energies). However, it is known that adiabatic energies provide better results when working with more stable molecules, so we chose to use adiabatic energies in order to get the best approximation.

Our results for the reactivity parameters of sodium selenite should enable more knowledge to be gained on this compound's interactions with other molecular systems, which should prove useful for biological applications.

Fukui functions were calculated because they can indicate the sites in sodium selenite that are favored in interactions with other molecular systems.

The Mulliken charge study predicted a negative value for O(2), so it is recommended that AIM should be used for selectivity characterization.

Acknowledgments D.B.J. and E.S. are researchers from CONACYT and CIAD, D.G.M. is a researcher from CONACYT and CIMAV, DH.G. is a researcher from CNyN at Universidad Nacional Autónoma de México (UNAM). A.F.H. is grateful for the doctoral scholarship granted by the Consejo Nacional de Ciencia y Tecnología (CONACYT).

References

1. Ximénez-Embún P, Alonso I, Madrid-Albarrán Y, Cámara C (2004) Establishment of selenium uptake and species distribution in lupine, Indian mustard, and sunflower plants. J Agric Food Chem 52(4):832–838
2. Zhu Y-G, Pilon-Smits EAH, Zhao F-J, Williams PN, Megharg AA (2009) Selenium in higher plants: understanding mechanisms for biofortification and phytoremediation. Trends Plant Science 14:436–442. doi:10.1016/j.tplants.2009.06.006
3. Rayman MP (2002) The argument for increasing selenium intake. Proc Nutr Soc 61:203–215
4. Diwadkar-Navsariwala V, Prins GS, Swanson SM, Birch LA, Ray VH, Hedayat S, Lantvit DL, Diamond AM (2006) Selenoprotein deficiency accelerates prostate carcinogenesis in a transgenic model. Proc Natl Acad Sci USA 103:8179–8184
5. Smkolji P, Pograje L, Hlaston-Ribic C, Stibilj V (2005) Selenium content in selected Slovenian foodstuffs and estimated daily intakes of selenium. Food Chem 90:691–697. doi:10.1016/j.foodchem.2004.04.028
6. Pedrero Z, Madrid Y, Cámara C (2006) Selenium species bioaccessibility in enriched radish (*Raphanus sativus*): a potential dietary source of selenium. J Agric Food Chem 54:2412–2417
7. Chen L, Yang F, Xu J, Yun H, Hu Q, Zhang Y, Pan G (2002) Determination of selenium concentration of rice in China and effect of fertilization of selenite and selenate on Se content of rice. J Agric Food Chem 50:5128–5130
8. Lyons GH, Stangoulis JCR, Gram RD (2004) Exploiting micronutrient interaction to optimize biofortification programs: the case for inclusion of selenium and iodine in the Harvest Plust programs. Nutr Rev 62:247–252
9. Abdo KM (1994) Toxicity Report Series Number 38. National Toxicology Program, Bethesda

10. Pehrson B, Ortman K, Madjid N, Trafikowska U (1999) The influence of dietary selenium as selenium yeast or sodium selenite on the concentration of selenium in the milk of Suckler cows and on the selenium status of their calves. J Anim Sci 77:3371–3376
11. Romero-Pérez A, García-García E, Zavaleta-Mancera A, Ramírez-Bribiesca JE, Revilla-Vázquez A, Hernández-Calva LM, López-Arellano R, Cruz-Monterrosa RG (2010) Designing and evaluation of sodium selenite nanoparticles in vitro to improve selenium absorption in ruminants. Vet Res Commun 34:71–79. doi:10.1007/s11259-009-9335-z
12. Li X, Liu Y, Deng F, Wang C, Qu S (2000) Microcalorimetric study of the toxic effect of sodium selenite on the mitochondria metabolism of *Carassius auratus* liver. Biol Trace Elem Res 77:261–271
13. Ting-Ming C, Fang-Yuan H, Cai-Min X, Bing-She H, Hua D, Lu Z, Xuan W, Yang Y, Hua-Zhen P, Zhi-Nan Z (2006) Distinct effects of different concentrations of sodium selenite on apoptosis, cell cycle, and gene expression profile in acute promyeloytic leukemia-derived NB4 cells. Ann Hematol 85:434–442. doi:10.1007/s00277-005-0046-4
14. Sharma S, Bansal A, Dhillon SK, Karaj S (2009) Comparative effects of selenate and selenite on growth and biochemical composition of rapeseed (*Brassica napus* L.) Dhillon. Plant Soil. doi:10.1007/s11104-009-0162-3
15. Sanuki S, Kojima T, Arai M, Nagaoka S, Majima H (1999) Photocatalytic reduction of selenate and selenite solutions using TiO_2. Metall Mater Trans B 30B:15–20. doi:10.1007/s11663-999-0002-0
16. Xiong G, Sullivan VS, Stair PC, Zajac GW, Trail SS, Kaduk JA, Golabb JT, Brazdil JF (2004) Effect of titanium substitution on the structure of $VSbO_4$ catalysts for propane ammoxidation. J Catal 230:317–326. doi:10.1016/j.jcat.11.046
17. Ding YC, Xiang AP, Xu M, Zhu WJ (2008) Electronic structures and optical properties of -Si_3N_4 doped with La. Physica B 403:2200–2206. doi:10.1016/j.physb.2007.11.025
18. Zhou X, Liu T, Zhang Q, Cheng F, Qiao H (2009) First-principles study of cadmium vacancy in $CdWO_4$ crystal. Solid State Sci 11:2071–2074. doi:10.1016/j.solidstatesciences.2009.09.006
19. Louail L, Haddadi K, Maouche D, Ali Sahraoui F, Hachemi A (2008) Electronic band structure of calcium selenide under pressure. Physica B 403:3022–3026
20. Gua W, Wang SY, Xu M, Chen YR, Chen LY, Jia Y (2009) Studies of the electronic and optical properties of BaMxO1_x (M = S, Se, Te) using first-principle calculations. Opt Commun 282:48–52. doi:10.1016/j.optcom.2008.09.077
21. Zhang H, Liu T, Zhang Q, Wang X, Guo X, Song M, Yin J (2009) First-principles study on electronic structures and color centers in $BaWO_4$ crystal with barium vacancy. Physica B 404:1538–1543. doi:10.1016/j.physb.2009.01.011
22. Verma VP (1999) A review of synthetic thermoanalytical, IR, Raman and X-ray studies on metal selenites. Thermochim Acta 327:63–102
23. Vlaev L, Tavlieva M, Barthel J (2007) Temperature and concentration dependences of the electrical conductance, diffuson and kinetic parameters of sodium selenite solutions in ordinary and heavy water. J Sol Chem 36:447–465. doi:10.1007/s10953-007-9125-6
24. Pronina NA, Kovshova YI, Popova VV, Lapin AB, Alekseeva SG, Baum RF, Mishina IM, Tsoglin LN (2002) The effect of selenite ions on growth and selenium accumulation in *Spirulina platensis*. Russ J Plant Physiol 49:235–241. doi:10.1023/A:1014809825140
25. Wang Y (2009) Differential effects of sodium selenite and nano-Se on growth performance, tissue Se distribution, and glutathione peroxidase activity of avian broiler. Biol Trace Elem Res 128:184–190. doi:10.1007/s12011-008-8264-y
26. Wickleder MS (2002) Sodium selenite, Na_2SeO_3. Acta Cryst E58: i103–i104
27. Altmann JA, Handy NC (1999) Evaluation of the performance of the HCTH exchange-correlation functional using a benchmark of sulfur compounds. Phys Chem Chem Phys 1:5529–5536
28. Hohenberg P, Kohn W (1964) Inhomogeneous electron gas. Phys Rev B 163:864–871. doi:10.1103/PhysRev.136.B864
29. Kohn W, Sham LJ (1965) Self-consistent equations including exchange and correlation effects. Phys Rev A 140:1133–A1138. doi:10.1103/PhysRev.140.A1133
30. Segall MD, Lindan PJD, Probert MJ, Pickard CJ, Hasnip PJ, Clark SJ, Payne MC (2002) First-principles simulation: ideas, illustrations and the CASTEP code. J Phys Condens Matter 14:2717–2744. doi:10.1088/0953-8984/14/11/301
31. Broyden CG (1970) The convergence of a class of double-rank minimization algorithms. 2: The new algorithms. J Inst Math Appl 6:222–231. doi:10.1093/imamat/6.3.222
32. Fletcher R (1970) A new approach to variable metric algorithms. Comput J 13:317–322. doi:10.1093/comjnl/13.3.317
33. Goldfarb D (1970) A family of variable-metric algorithms derived by variational means. Math Comput 24:23–26
34. Shanno DF (1970) Conditioning of quasi-Newton methods for function minimization. Math Comput 24:647–656
35. Perdew JP, Wang Y (1992) Accurate and simple analytic representation of the electron-gas correlation energy. Phys Rev B 45:13244–13249. doi:10.1103/PhysRevB.45.13244
36. Accelrys Software Inc. (2008) Materials Studio modeling, CASTEP code, release 4.4. Accelrys Software Inc., San Diego
37. Vanderbilt D (1990) Soft self-consistent pseudopotentials in generalized eigenvalue formalism. Phys Rev B 41:7892–7895. doi:10.1103/PhysRevB.41.7892
38. Accelrys Software Inc. (2008) Materials Studio release notes, release 4.4. Accelrys Software Inc., San Diego
39. Frisch MJ, Trucks GW, Schlegel HB, Scuseria GE, Robb MA, Cheeseman JR, Montgomery JA Jr, Vreven T, Kudin KN, Burant JC, Millam JM, Iyengar SS, Tomasi J, Barone V, Mennucci B, Cossi M, Scalmani G, Rega N, Petersson GA, Nakatsuji H, Hada M, Ehara M, Toyota K, Fukuda R, Hasegawa J, Ishida M, Nakajima T, Honda Y, Kitao O, Nakai H, Klene M, Li X, Knox JE, Hratchian HP, Cross JB, Bakken V, Adamo C, Jaramillo J, Gomperts R, Stratmann RE, Yazyev O, Austin AJ, Cammi R, Pomelli C, Ochterski JW, Ayala PY, Morokuma K, Voth GA, Salvador P, Dannenberg JJ, Zakrzewski VG, Dapprich S, Daniels AD, Strain MC, Farkas O, Malick DK, Rabuck AD, Raghavachari K, Foresman JB, Ortiz JV, Cui Q, Baboul AG, Clifford S, Cioslowski J, Stefanov BB, Liu G, Liashenko A, Piskorz P, Komaromi I, Martin RL, Fox DJ, Keith T, Al-Laham MA, Peng CY, Nanayakkara A, Challacombe M, Gill PMW, Johnson B, Chen W, Wong MW, Gonzalez C, Pople JA (2004) Gaussian 03, revision C.02. Gaussian Inc., Wallingford
40. Hamprecht FA, Cohem AJ, Tozer DJ, Handy NC (1998) Development and assessment of new exchange-correlation functional. J Chem Phys 109:6264. doi:10.1063/1.477267
41. Boese AD, Handy NC (2000) New generalized gradient approximation functional. J Chem Phys 112:1670–1678. doi:10.1063/1.480732
42. Boese AD, Martin JML (2004) Development of novel density functionals for thermochemical kinetics. J Chem Phys 121:3405–3416. doi:10.1063/1.1774975
43. Godbout N, Salahub DR, Andzelm J, Wimmer E (1992) Optimization of Gaussian-type basis sets for local spin density functional calculations. Part I. Boron through neon, optimization technique and validation. Can J Chem 70:560–571. doi:10.1139/v92-079
44. Coquet R, Mizuki T, Iwasawa Y (2007) Energy-gaining formation and catalytic behavior of active structures in a SiO_2-supported unsaturated Ru complex catalyst for alkene epoxidation by DFT calculations. Phys Chem Chem Phys 9:6040–6046. doi:10.1039/b710714e
45. Parr RG, Yang W (1984) Density functional approach to the frontier-electron theory of chemical reactivity. J Am Chem Soc 106:4049–4050. doi:10.1021/ja00326a036
46. Mulliken RS (1955) Electronic population analysis on LCAO-MO molecular wave functions. J Chem Phys 23:1833–1840. doi:10.1063/1.1740588

47. Mulliken RS (1962) Criteria for the construction of good self-consistent field molecular orbital wavefunctions and the significance of LCAO-MO population analysis. J Chem Phys 36:3428–3439
48. Bader RFW (1990) Atoms in molecules. A quantum theory. Oxford University Press, Oxford
49. Parr RG, Donnelly RA, Levy M, Palke WE (1978) Electronegativity: the density functional viewpoint. J Chem Phys 68:3801–3807. doi:10.1063/1.436185
50. Toro-Labbé A (1999) Characterization of chemical reactions from the profiles of energy, chemical potential and hardness. J Phys Chem A 103:4398–4403. doi:10.1021/jp984187g